



## Heterogeneous Catalyst based on Nickel Modified into Indonesian Natural Zeolite in Green Diesel Production from Crude Palm Oil

Fauzan Ibnu Prihadiyono<sup>1</sup>, Witri Wahyu Lestari<sup>1\*</sup>, Riandy Putra<sup>1,2</sup>, Arifti Nur Laily Aqna<sup>1</sup>, Indri Sri Cahyani<sup>1</sup>, and Grandprix T.M. Kadja<sup>3,4,5</sup>

<sup>1</sup>Chemistry Department, Faculty of Mathematics and Natural Sciences, Universitas Sebelas Maret, Jl. Ir. Sutami No.36A, Ketingan–Jebres Surakarta, Central Java, Indonesia, 57126

<sup>2</sup>Department of Chemistry, Faculty of Mathematics and Natural Sciences, Universitas Palangka Raya, Kampus UPR Tunjung Nyaho, Palangka Raya, 73111, Indonesia

<sup>3</sup>Division of Inorganic and Physical Chemistry, Faculty of Mathematics and Natural Sciences, Institut Teknologi Bandung, Jalan Ganesha no. 10, Bandung 40132, Indonesia

<sup>4</sup>Center for Catalysis and Reaction Engineering, Institut Teknologi Bandung, Jalan Ganesha no. 10, Bandung 40132, Indonesia

<sup>5</sup>Research Center for Nanosciences and Nanotechnology, Institut Teknologi Bandung, Jalan Ganesha no. 10, Bandung 40132, Indonesia

**Abstract.** Green diesel is an alternative renewable and environmentally friendly fuel in the transportation sector. This study aimed to modify Indonesian natural zeolite (NZ) with nickel and apply it as a catalyst in green diesel production from crude palm oil (CPO). The materials were prepared with different Ni content of 3, 5, and 10 wt.% and characterized in detail using X-Ray Diffraction (XRD), Scanning Electron Microscope (SEM), Transmission Electron Microscope (TEM), Fourier Transform infra-red Spectroscopy (FTIR), and Surface Area Analyzer (SAA). Catalytic tests were performed in a batch reactor at a temperature of 375 °C and a pressure of 12 bar for 2 hours. Gas Chromatography-Mass Spectrometry (GC-MS) analysis was used to determine the liquid product. Based on XRD analysis, the crystallinity of materials tends to decrease after being modified with Ni. Concomitantly, the presence of Ni was indicated by new peaks with increasing intensity at  $2\theta = 44^\circ, 55^\circ,$  and  $76^\circ$ . SEM analysis shows morphological changes in materials with decreasing particle sizes. The presence of Ni is also known by the presence of small spheres scattered in the material and black shades observed in TEM analysis. Based on IUPAC, the resulting isotherm graph is categorized as type I with type IV loop hysteresis and classified as micropore with an average pore size is  $<2$  nm. The highest activity and selectivity on  $C_{15}$  were achieved up to 77.34% and 53.11% when 3% of Ni modified NZ was applied as Catalyst compared to NZ, and other Ni modified NZ.

**Keywords:** Crude Palm Oil; Green Diesel; Hydrodeoxygenation; Natural zeolite; Nickel

### 1. Introduction

Energy consumption is increasing drastically, along with the various increasing sectors of life. The major energy consumption area is the transportation sector that is still limited to non-renewable sources such as fossil fuels and would soon be exhausted. Therefore, exploring new renewable sources and clean energy, e.g., geothermal, solar system, the

\*Corresponding author's email: [witri@mipa.uns.ac.id](mailto:witri@mipa.uns.ac.id), Tel.: +62-271- 663375; Fax: +62-27-1663375  
doi: [10.14716/ijtech.v13i4.4695](https://doi.org/10.14716/ijtech.v13i4.4695)

hydroelectric, wind, and bioenergy from plants and animals, would have great impact (Ameen et al., 2017).

Biofuel based on vegetable oils, such as palm oil, are a potential alternative energy source because of their abundance, renewability, and easy processing (Ameen et al., 2019; Mardiana et al., 2022). Palm oil comprises a mixture of mono-alkyl esters from a long chain of fatty acids (mostly 17–19 carbon atoms), which can be converted into biodiesel through a catalytic process (Hermida et al., 2015). However, biodiesel is constrained with those by oxygenating products, which might cause damage to the diesel engines. The oxidative nature of biodiesel is determined by the presence of C=O and C=C bonds within the products and toxic emissions of nitrogen oxide (NO<sub>x</sub>) (Ajala et al., 2015; Putra et al., 2018). Therefore, further research is required to develop green diesel with free-oxygen and n-paraffin (C<sub>x</sub>H<sub>y</sub>) components with cetane numbers approaching 100. In addition, diesel-range alkanes are obtained as the final products with high stability and eco-friendly (Alvarez-galvan et al., 2019; Chen et al., 2018; Muharam & Soedarsono, 2020).

The production of green diesel can be achieved through the hydrodeoxygenation (HDO) reaction that aims to remove oxygen to reduce biodiesel's oxidative levels (Yuswan et al., 2018; Shafaghat et al., 2018). The HDO reaction requires high temperature and pressure. Therefore, the HDO reaction needs a catalyst that assists in the production of second-generation biodiesel through faster and more effective reactions. However, the development of catalysts for the HDO reaction is constrained by the resistance of the catalyst material to high temperatures and low product selectivity (Lani et al., 2016). Natural zeolite can be a heterogeneous catalyst in the HDO reaction because it contains active acidic sites and robust physicochemical stability (Arun et al., 2015). In addition, natural zeolites exhibit high thermal stability, organic solvents resistance, low-cost, and non-toxicity (Primo & Garcia, 2014). The natural zeolite could be activated through physical and chemical treatments to remove impurities and enhance the amount of pore and zeolite specific surface area (Setiawan & Mahatmanti, 2018). Furthermore, the selectivity of catalytic reactions also can be increased through the loading of metals on the supporting material (Inokawa et al., 2010; Yulizar et al., 2016). As a result, the catalytic performance can be improved by increasing the active site of the Catalyst. The selection of metals for the HDO process is a challenge for current research.

The noble metal catalysts such as Pd (Yang et al., 2017), Ru (Dwiatmoko et al., 2019), and Pt (Yang et al., 2015) have also been used for HDO catalytic activity at low temperatures, but the high price of these metals is detrimental for the production cost-effectiveness. Thus, considering the low stability and high cost of these precious metal catalysts, it is imperative to develop alternative non-noble metal-based catalyst for HDO (Chen et al., 2018; Hachemi et al., 2017). Transition metals can be used as alternative catalysts such as cobalt (Co), iron (Fe), molybdenum (Mo), and nickel (Ni) (Hongloi et al., 2019). Nickel is an attractive metal due to its high availability, excellent hydrogenation capability, and good stability (Gamliel et al., 2018). Ni has better properties than other transition metals (Cu, Co, and Fe) concerning atomic volume, structure, and atomic radius. The d-electrons and the density level of energy around the lattice plane of Ni are higher than other transition metals, thus affecting catalytic properties (Chen et al., 2018; De et al., 2016).

Nickel-based heterogeneous catalysts are the most widely shown good performance in deoxygenation reaction (Hongloi et al., 2019). It has been reported that hydrogen molecules could be trapped in the surface defects of nickel (Liu et al., 2013). Moreover, the electronic properties of Ni metal allow similar activity reactions to those of noble metals (Pd or Pt), such as the selective C–C or C–H cleavage for hydrocarbon reaction (De et al., 2016; Hongloi et al., 2019). Kaewmeesri et al. (2015) reported Ni/γ-Al<sub>2</sub>O<sub>3</sub> catalysts for the methyl

palmitate HDO reaction with a conversion of 60% and alkane C<sub>10</sub>–C<sub>12</sub> selectivity of 58%. Research conducted by [Ma and Zhao \(2015\)](#) using nickel–metal nanoparticles embedded in Hierarchica Beta Zeolite (HBEA) zeolite catalyst showed the total yields of n–octadecane (C<sub>18</sub>) kept stable at 70 wt% after one h. By using palm oil as feedstocks, [Susanto et al. \(2016\)](#) tested NiMo/ZAL (Clinoptilolite type) catalyst for hydrodeoxygenation reaction under hydrogen pressure of 15 bar and temperature of 375°C. The result showed that the renewable diesel yield (C<sub>13</sub>–C<sub>19</sub>) produced a conversion of around 80.87% and selectivity of 52.78%. At the same time, the Ni/SAPO–11 catalyst used to convert palm oil to the hydrodeoxygenation reaction obtained an alkane yield (C<sub>15</sub>–C<sub>18</sub>) of around 70% conversion and 80% isomerization selectivity of long alkanes ([Liu et al., 2014](#)).

According to [Hongloi et al. \(2019\)](#), Ni/ZrO<sub>2</sub> could convert palmitic acid to n–alkane as the main composition in green diesel (C<sub>15</sub>–C<sub>18</sub>) of 98.33% and n–pentadecane (C<sub>15</sub>) with selectivity by 76%. [Hachemi et al. \(2017\)](#) also studied sulfur-free Ni supported on H–Y zeolites γ–Al<sub>2</sub>O<sub>3</sub>, and SiO<sub>2</sub> synthesized by the wet impregnation method. They were tested in hydrodeoxygenation (HDO) of stearic acid. The result showed that C<sub>17</sub> was the main product from HDO of stearic acid over Ni/H–Y zeolites, Ni/γ–Al<sub>2</sub>O<sub>3</sub>, and Ni/SiO<sub>2</sub> representing 50% of products obtained from HDO. Similar research conducted by [Yang et al. \(2012\)](#) reported the supported Ni<sub>2</sub>P/SBA–15 catalyst was tested for the HDO of methyl oleate produced n–alkanes in the C<sub>15</sub>–C<sub>18</sub> range which are formed from a feedstock composed mainly of C<sub>18</sub> (80%).

The utilization of NZ modified by Fe in HDO reaction of refined palm oil was firstly investigated by our group ([Putra et al., 2018](#)) and showed high conversion up 89% and selectivity of C<sub>15</sub>–C<sub>18</sub> up to 76%. The selection of metal embedded into NZ play a crucial role in the activity and selectivity of Catalyst. So far, modification of NZ with Ni as Catalyst for green diesel production has never been studied. Herein, this study will investigate the effect of Ni with different metal loading (3, 5, and 10 wt.%) modified into NZ in catalyzing green diesel production from crude palm oil.

## 2. Methods

### 2.1. Materials

The NZ was obtained from Wonosari, Klaten, and Central Java (particle size 170/240 mesh). Demineralization water, Nickel (II), Acetylacetonate (Ni(acac)<sub>2</sub>) (Sigma Aldrich, 95%), and chloroform (type for analysis, Merck) were used as purchased. Pure nitrogen and hydrogen gas (99% ultra-high purity) were commercially provided by PT. Samator Indonesia and Crude Palm Oil (CPO) was obtained from PT. Salim Ivomas Pratama, Tbk.

### 2.2. Materials characterization

The X-ray diffraction (XRD) Rigaku Miniflex 600 Benchop operated at 40 kV, and 30 mA with Cu–Kα radiation was used to identify the phase purity and crystallinity of the materials. The change of functional groups present in materials and green diesel products were observed using the Fourier Transform Infrared (FTIR) spectroscopy Shimadzu IR Prestige–21. Pore size and surface area of the materials were measured with Quadradsorb Evo N<sub>2</sub>. The distribution of impregnated nickel metals into NZ was observed by JEM–1400 Transmission Electron Microscopy (TEM). In addition, the morphological structure of the materials was also identified by FEI Inspect–S50 Scanning Electron Microscopy (SEM).

### 2.3. Preparation of Natural Zeolite

Natural zeolite from Klaten, Central Java, was treated by soaking the zeolite in demineralized water and stirred for 24 hours at room temperature, filtered, and dried in an oven at 100 °C for 24 hours then mashed with a sieving size of 200 mesh.

### 2.4. Metal Impregnation

The Ni/NZ was prepared using the wetness impregnation method. Ni(acac)<sub>2</sub> was dissolved in 20 ml of chloroform with a weight variation of 3, 5, and 10 wt%. This solution was added dropwise into the zeolite and then stirred for 2 hours, 600 rpm. The obtained mixture was evaporated to remove the solvent. Finally, the catalyst material was reduced to 550 °C under hydrogen flow (10 mL/min) for 2 hours.

### 2.5. Catalytic Test

The hydrodeoxygenation reaction was carried out in a 100 cm<sup>3</sup> hydrotreating autoclave reactor (batch reactor) as shown in Figure 1, equipped with a stirrer, condenser, and pump. The autoclave was purged with nitrogen for 15 minutes, and the reaction was adjusted at 12 bar atm H<sub>2</sub>, 375 °C, and stirred for 2 hours. The reaction temperature was cooled and allowed to stand for 5 hours to reach room temperature. The batch autoclave reactor was equipped with a condenser and a distillate tube aiming to drain steam and other gas products produced during the catalytic process. The product was then distilled according to the ASTM–D86 method. The liquid phase product was identified by Gas chromatography–mass spectroscopy (GC–MS, QP2010S–Shimadzu, with an autosampler and a 5975C mass selective detector) equipped with an HP-INNOWax capillary column (30 m × 0.25 mm × 0.20 μm film thickness). The measurements started at a 40°C hold for 0.5 minutes rising at 8°C/min to a 195°C hold for 0 minutes and finally rising 1°C/min to 225°C and holding for 22 minutes. Helium was used as the carrier gas (1.8614 mL/minute), and an injection volume of 1 μL were used to identify the components in the HDO product.

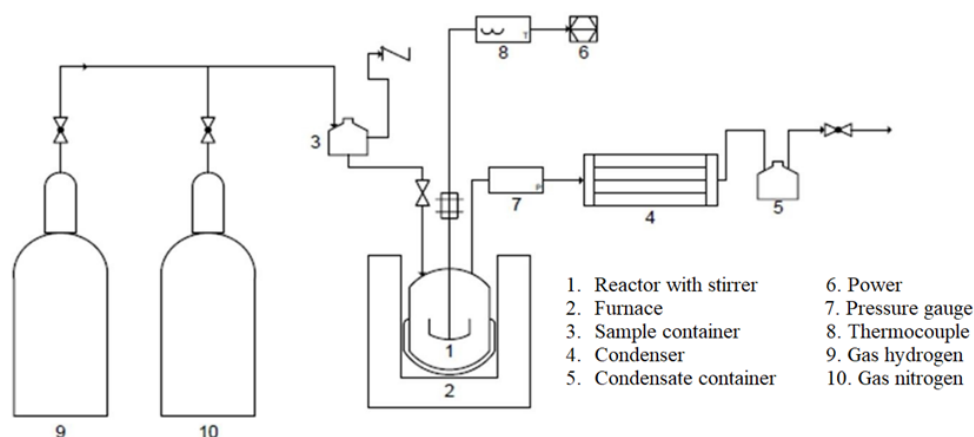


**Figure 1** Experiment set-up and apparatus of Hydrodeoxygenation (HDO) reactor

### 2.6 Evaluation of HDO Products

The conversion and selectivity of Catalyst were defined according to the equations (1) and (2) refer to Liu *et al.* (2016)

$$C = 100\% - C_{(TG)}, \quad (1)$$

with  $C_{(TG)}$  is the concentration of triglycerides (%) in the product oil determined by GC analysis. The selectivity of C<sub>15</sub>–C<sub>18</sub> hydrocarbon was calculated as:

$$S = Y_i / C \times 100\%, \quad (2)$$

with  $Y_i$  is the yield of the C<sub>15</sub>–C<sub>18</sub> hydrocarbon (%), determined by GC analysis, and C is the conversion of palm oil (%) calculated with Eq. (1).

### 3. Results and Discussion

#### 3.1. Materials Characterization

XRD diffractograms of NZ (Figure 2) showed that the material consists of mordenite and clinoptilolite phases following the standard pattern ICSD #068448 and #072712. The refinement analysis using the Le Bail method showed that the content of mordenite (MOR) and clinoptilolite (HEU) phases is 56.21% and 43.79%. This value is in line with research conducted by Putra et al. (2018), who used the NZ pattern with accepted values by residual phase ( $R_p$ ) and residual weight phase ( $R_{wp}$ ). Based on the X-Ray diffractogram of Ni/NZ (Figure 2), the majority of the pattern showed no structural changes could be observed even after metal impregnation, indicating that the structure of the NZ remains stable.

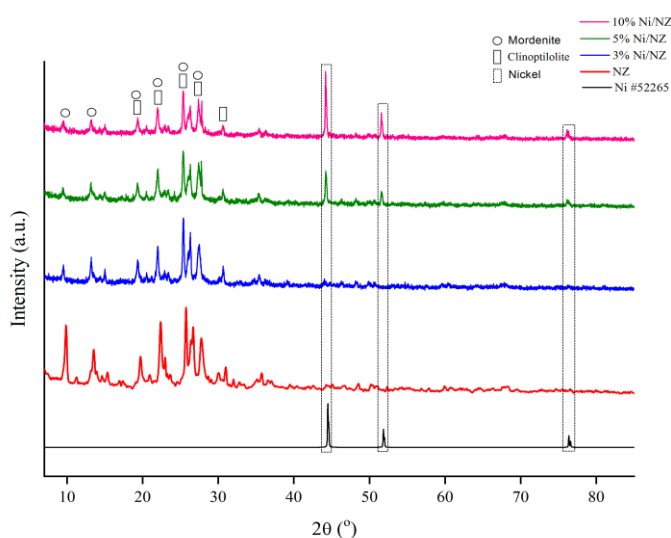


**Figure 2** X-ray Diffractogram of NZ and Ni/NZ samples

The diffraction peaks at  $2\theta = 44$ ,  $55$ , and  $76^\circ$  showed an increase in intensity which represented nickel metal (ICSD #52265) corresponding to the (111), (200), and (220) crystallographic planes of the face-centered cubic Ni phase, respectively. The increase of the three diffractograms showed a greater percentage of the existing Ni phase, in agreement with the results reported by Zuo et al. (2012) and Srifa et al. (2018). Furthermore, the stronger diffraction peaks at  $2\theta = 44^\circ$  were found in 10 wt% Ni/NZ, suggesting the complete reduction of  $\text{Ni}(\text{acac})_2$  to metallic Ni at  $550^\circ\text{C}$ . In addition, the XRD results showed the relative crystallinity of the materials tended to decrease when the nickel metals were loaded into NZ. However, the comparison of the 68% relative crystallinities of 5% Ni/NZ with the 56% relative crystallinity of 3% Ni/NZ indicated that the 5% Ni/NZ exhibit a good crystal state after the introduction of Ni metal. The comparison of the relative crystallinity of ZA and Ni/NZ are listed in Table 1.

**Table 1** Relative crystallinities of the NZ and Ni/NZ

Sample	Rel. Intensity (%)	Value %
NZ	698.60	100
3% Ni/NZ	397.22	56.85
5% Ni/NZ	480.65	68.80
10% Ni/NZ	340.31	48.71

FTIR spectra of the materials are presented in Figure 3. The absorption peak of O–H bending in NZ appears at wavelength number  $1634\text{ cm}^{-1}$ , while O–H stretching of silanol

groups was observed at  $3418\text{ cm}^{-1}$ . Absorption peaks of Si–O–Si asymmetric and symmetric stretching were detected at  $1047\text{ cm}^{-1}$  and  $796\text{ cm}^{-1}$ , respectively. After being modified with Ni metal, the spectra did not change significantly, indicating that there are no chemical interactions of Ni metal and NZ as supporting material.

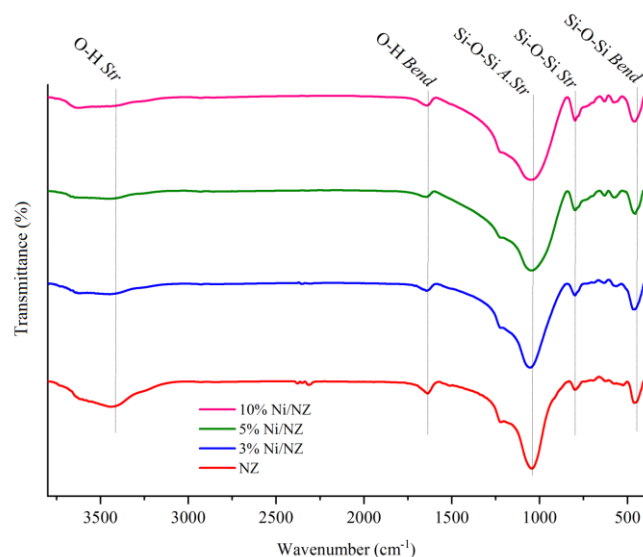


**Figure 3** FTIR spectra of NZ and Ni/NZ samples

The interpretation of total surface area was calculated using the Brunauer–Emmett–Teller (BET) equation with relative partial pressure  $P/P_0 = 0.05–0.03$ . The total pore volume and pore size distribution were calculated using Barret–Joyner–Hallenda (BJH) method, as shown in Table 2. The surface area of NZ increased after the impregnation of nickel-metal as the trend increased of the Ni-loading. Modification with nickel might cover the pores, thereby increasing the NZ material’s surface area. In addition, metal impregnation did not damage the micropore structure of the NZ material, as evidenced by the change in pore size (less than 2 nm) (Hou et al., 2018). The surface area and pore size increased when five wt.% Ni and ten wt.% Ni was deposited on the NZ material with a major contribution from the external surface because of the presence of the Ni particles (Chen et al., 2016). However, when 3 wt.% Ni metal was loaded, the specific surface area and pore size decreased due to Ni metal convergence on the NZ support, and the pores might be blocked by Ni particles (Hongloi et al., 2019; Srifa et al., 2015). According to the IUPAC classification, the  $N_2$  adsorption-desorption isotherms profile of 3% Ni/NZ, 5%Ni/NZ, and 10% Ni/NZ showed type I with type IV behaviors hysteresis loop. Based on the following classification corresponded to micropore material properties with an average pore size of less than 2 nm (in Figure 4) (Thommes et al., 2015).

**Table 2** Surface area, Pore Volume, and Pore size of NZ and Ni/NZ samples

Sample	Surface Area (m <sup>2</sup> /g)	Total Pore Volume (cc/g)	Pore Size (nm)
NZ	26	0.07	1.95
3% Ni/NZ	16	0.13	1.96
5% Ni/NZ	37	0.09	1.98
10% Ni/NZ	122	0.22	1.89

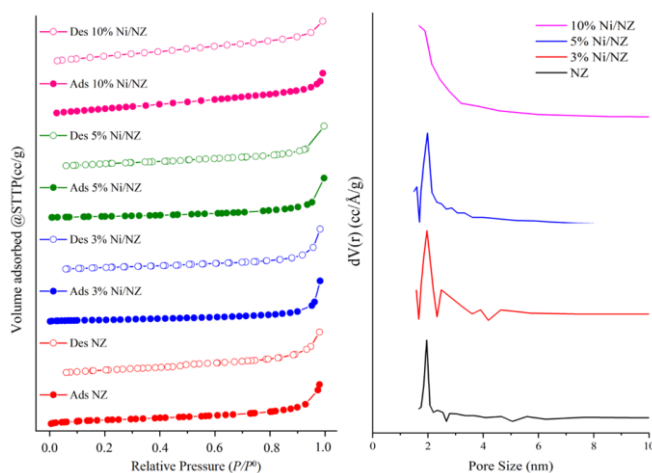


**Figure 4** Nitrogen sorption isotherm and pore distribution of NZ and Ni/NZ

Based on observation using SEM in Figure 5 (a), the morphology of NZ showed an irregular shape and had a rough surface with an average particle size of ca. 3  $\mu\text{m}$ . Therefore, the addition of Ni-metal in figures 5 (b), (c), and (d) did not significantly change the morphology, and Ni particles revealed the uniform dispersion (Hongloi et al., 2019). The high percentage of nickel-loading leads to produce smaller particle sizes with a distribution size of 1–2  $\mu\text{m}$  (in Figure 5). It was found that the particles of Ni were small dispersed, and the suitable concentration weight of nickel impregnated on NZ was shown by EDX. The SEM analysis confirms the XRD analysis that Ni-metals are homogeneously filled and dispersed on the porous NZ material.

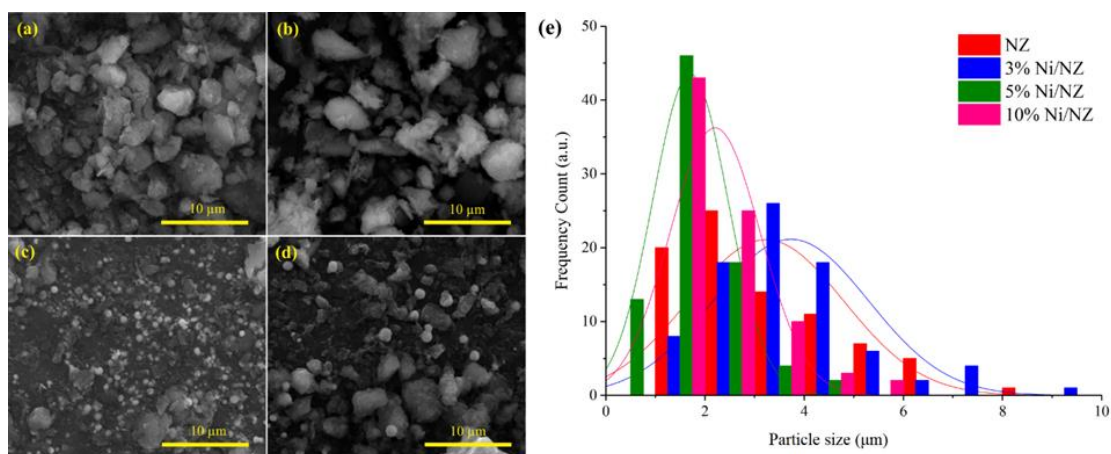


**Figure 5** SEM images of (a) NZ and Ni/NZ (b) 3 wt.% (c) 5 wt.% (d) 10 wt.% and (e) histogram of the particle size distribution

The nickel-size distributions on NZ as supporting material was visualized by TEM analysis (Figure 6). The brighter dots display the location of NZ material, while small spheres scattered with darker dots show the loaded Ni metal nanoparticles. Figure 6 (a) and (b) display Ni-metal dispersion on the NZ with an average crystallite size of 1.5 nm, in accordance with the XRD analysis calculated with Scherrer's equation. Moreover, Figure 6 (c) showed medium dots with an average crystallite size of 9.3 nm, which is possible due to agglomeration as depicted in Figure 5 (d), in which the metal loaded with 10 wt.% Ni has a greater size than other modifications. These results suggest that promoting the high nickel-metal loading effect of this study is also in good agreement with XRF analysis (Table 3).

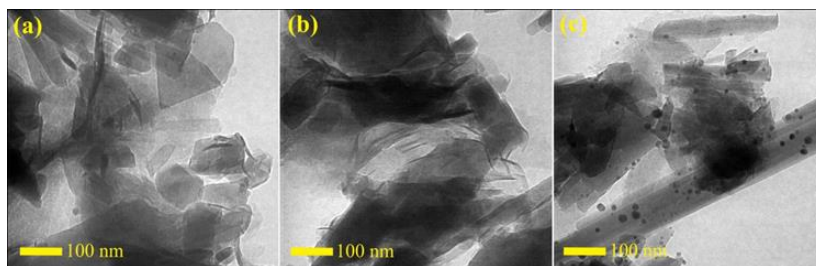


**Figure 6** TEM images of Ni/NZ: (a) 3 wt.% (b) 5 wt.% and (c) 10 wt.%

**Table 3** Element distribution of catalyst materials from XRF characterization (wt%)

Compound	NZ	3% Ni/NZ	5% Ni/NZ	10% Ni/NZ
O	51.23	50.85	51.37	49.20
Si	33.08	33.90	31.06	29.75
Al	5.34	5.72	4.90	4.69
Ca	5.87	3.71	3.70	3.55
Na	4.48	2.22	2.99	2.86
Ni	n.d.	3.60	5.97	9.95

n.a. = not detected

### 3.2. Catalytic tests

According to GC-MS analysis, the liquid products of the hydrogenation reaction showed the diesel-hydrocarbon fraction as a major product which consisted of long-chain *n*-alkanes (C<sub>15</sub>-C<sub>18</sub>) as shown in Table 4. The higher loadings of Ni-metals do not show an increase in the percentage of HDO products. It may be the catalyst has an agglomeration effect so that influencing activity and selectivity with the reactants gradually decreased. The HDO products corresponded to our previous work (Putra et al., 2018) where Fe modified on NZ material was used as the Catalyst in the hydrogenation of refined palm oil. They reported 58% and 89% conversion to C<sub>15</sub>-C<sub>18</sub> hydrocarbons when NZ and Fe modified NZ (Fe/NZ), respectively, agreed with these results. The HDO reaction for triglycerides carried out by Taromi and Kaliaguine (2018) using a Ni/γ-Alumina catalyst with impregnation and sol-gel techniques showed liquid products mostly consisted of C<sub>15</sub>-C<sub>18</sub> hydrocarbons reached up to 70-80% yield. In addition, the use of Ni-based metal catalysts was also carried out by Srifa et al. (2018) applied to Ni/γ-Al<sub>2</sub>O<sub>3</sub> with triglyceride reactants. The main products are *n*-alkanes C<sub>15</sub> and C<sub>17</sub> with up to 80% conversion. Based on Table 4, it can be noted that the most abundant hydrocarbon products were pentadecane (C<sub>15</sub>) and heptadecane (C<sub>17</sub>). It can be suggested that the C<sub>15</sub> and C<sub>17</sub> products generated through the decarbonylation (DCO) or decarboxylation (DCO<sub>2</sub>) routes were the same as those indicated by Deliy et al. (2014) and Xin et al. (2016), who used a Ni-based catalyst.

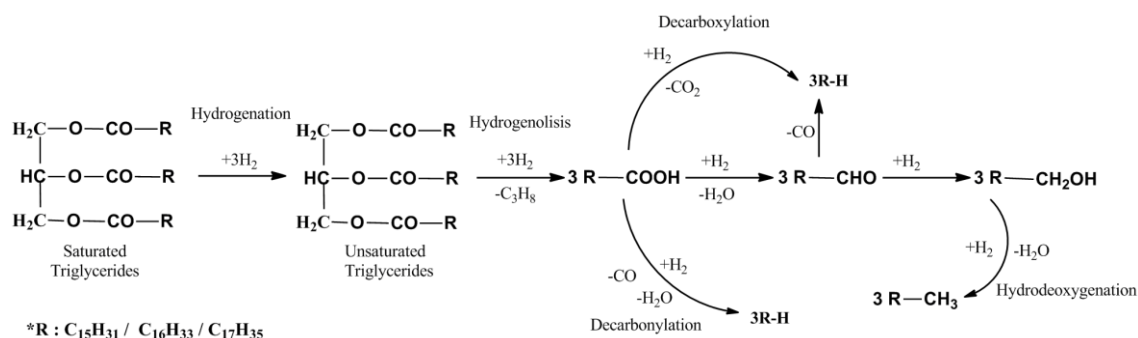


**Figure 7** Prediction of the deoxygenation reaction mechanism of crude palm oil through decarboxylation, decarbonylation, and hydrodeoxygenation reaction (Hongloi et al., 2019; Srifa et al., 2018)

The deoxygenation process was involved in 3 steps, namely hydrodeoxygenation (HDO), decarboxylation ( $\text{DCO}_2$ ), and decarbonylation (DCO). Crude palm oil contains various acids such as oleic acid, palmitic acid, and stearic acid. So, crude palm oil's deoxygenation process tends to react with those various acids. The mechanism of deoxygenation reaction that may occur for these studies in crude palm oil using a nickel-metal catalyst is described in Figure 7. According to Gousi et al. (2017), the generating of nickel-based catalysts applied the decarbonylation (DCO) process as the main pathway for deoxygenation. Firstly, the deoxygenation of fatty acids includes hydrogenation of C=C double bonds (unsaturated fat chains) followed by hydrogenolysis of oxygen bonds to saturated fatty acids to alkanes chain. The DCO pathway i.e.,  $\text{H}_2$  is first dissociated over Ni sites, and the dissociated H combines with the OH of palmitic acid (the most content in crude palm oil) to form  $\text{H}_2\text{O}$  generating aldehydes group as an intermediate. Finally, the intermediate is further converted to pentadecane by the DCO process (Xin et al., 2016). Another route may be involved; the carboxylic group was substituted and adsorbed on the oxygen vacancy sites on NZ then, displacement of the  $\alpha$ -Hydrogen with a removal of oxygen atom occurred. After that, Ni metal spilled over the hydrogen atoms to palmitic acid, producing  $\text{C}_{15}$  normal alkane (*n*-pentadecane) by DCO (Hongloi et al., 2019). The oxygen removal resulting from the HDO reaction can be seen in the product distribution in Figure 8. Based on the results, the presence of Ni metal can increase the deoxygenation properties of natural zeolites which are known to decrease the oxygenate fraction. The optimal reduction is achieved when using a 3 wt.% Ni/NZ catalyst.

It was noted that the selectivity of *n*-pentadecane significantly increased with a 3 wt.% Ni catalyst; thus, the high-grade diesel was obtained. The highest selectivity of *n*- $\text{C}_{15}$  was 53.12% obtained over the 3 wt.% Ni catalyst, as shown in Figure 8. This could indicate that the 3 wt.% Ni may be more stable than the other catalysts. Our previous studies (Putra et al., 2018) have proven that NZ modified with 3 wt.% Fe metal has a significant effect and reached an optimum 59.19% yield for selectivity of *n*- $\text{C}_{15}$ . These different results may influence by metal-oxygen bond strengths for catalysts used (Robinson et al., 2016). It is known that the bond strength of Fe-O (exophilic metal) was  $407 \text{ kJ mol}^{-1}$  provide strongly binds the oxygen to the surface of Fe/NZ through removing oxygen for selectivity to C-O with highly selective DCO/ $\text{DCO}_2$  reactions. Since the crude palm oil used in this study was mainly composed of  $\text{C}_{16}$  and  $\text{C}_{18}$  fatty acids. Furthermore, the bond strength of Ni-O (hydrogenating metal) with  $366 \text{ kJ mol}^{-1}$  preferentially follows the hydrogenation route to *n*- $\text{C}_{16}$  (9.74%) (3wt.% Ni) and  $\text{C}_{18}$  (0.89%) (3wt.% Ni) was higher than our previous studies (Putra et al., 2018).

Moreover, an increase in the Ni loading to 10 wt.% showed the lowest selectivity of *n*- $\text{C}_{15}$  (40.84%). This indicated a deactivation process on 10 wt.% Ni/NZ occurred which might be due to inaccessible pore or pore-blocking by too much Nickel. This phenomenon is supported by the pore size distribution data presented in Figure 4. This observation is in good agreement with Hongloi et al. (2019), and Chen et al. (2016) found that deactivation with 10 wt.% Ni/HZSM-5 catalyst was used. In addition, the hydrogenation of carboxylic acid groups might be converted into aldehydes as intermediates, then further hydrogenated to alcohol, and the HDO process occurred to remove O-H in alcohol by splitting the C-O bond directly to release  $\text{H}_2\text{O}$ . Moreover, decarboxylation can also occur immediately by removing carboxylic groups by cleavage of C-C bonds to release carbon dioxide (Gousi et al., 2017; Hongloi et al., 2019).

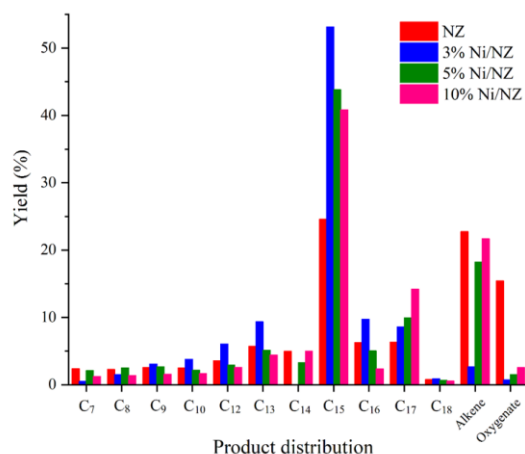


**Figure 8** Liquid yield product distribution of NZ and Ni/NZ catalyst in the HDO reaction of crude palm oil at 375 °C, 12 bar H<sub>2</sub>, and 2 h.

Based on Figure 8, it can be seen that the percentage of conversion to hydrocarbon products has increased after using an impregnated catalyst. The increase in the optimum conversion percentage is known in the addition of 3 wt.% nickel metal, which is 77.34%. These results are also supported by FTIR analysis. A decrease in the peak at the wavenumber around 1700 cm<sup>-1</sup> indicates a decrease in the C=O bond. This confirmed the results of the product distribution showed the decrease in oxygenating compounds after a catalytic reaction. The decrease in oxygen content can also be seen through a very significant change in the absorption peak around 1000–1250 cm<sup>-1</sup> represents a C–O bond. The HDO efficiency indicated by reducing the intensity of the transmittance ratio (C=O/C–H) reflects the decrease in oxygen content (Table 4). In these results the transmittance ratio of C=O/C–H in CPO was about 0.98, decreased to 0.44, 0.42, 0.81, and 0.79 when NZ, 3%Ni/NZ, 5% Ni/NZ, and 10% Ni/NZ, respectively, were used.

**Table 4** The transmittance ratio of C=O/C–H from HDO product catalyzed by NZ and Ni/NZ compared to starting material analyzed by FTIR spectroscopy

Catalyst	% T	% T	% Transmittance Ratio C=O/C–H
	C=O (1711 cm <sup>-1</sup> )	C–H (2854 cm <sup>-1</sup> )	
CPO (starting material)	76.62	77.63	0.98
NZ	36.93	83.38	0.44
3% Ni/NZ	35.19	82.79	0.42
5% Ni/NZ	69.69	86.43	0.81
10% Ni/NZ	67.87	84.87	0.79

#### 4. Conclusions

In this study, NZ shows suitability with the simulated pattern of MOR and HEU phases. The presence of Ni metal nanoparticles on NZ as supporting material had no significant influence on the chemical structure of zeolite but changed the morphology and decreased the crystallinity. Variation of Ni–metal loading increase the surface area and pore volume. Catalytic test of Ni/NZ material in converting crude palm oil to C<sub>15</sub>–C<sub>18</sub> as the main composition in green diesel achieved high selectivity up to 53.11%. Decarboxylation and decarbonylation were simulated as the main pathway reactions, which were dominated by the C<sub>15</sub> hydrocarbons chain. Finally, Ni/NZ exhibited a synergistic effect in selectivity to green diesel production from crude palm oil, showing its promising catalytic application.

## Acknowledgements

The authors acknowledge the financial support from the Ministry of Research, Technology, and Higher Education of the Republic of Indonesia through the Student Creativity Program (PKM-PE) 2018. Moreover, WWL would also like to acknowledge L'Oréal-UNESCO for Women in Science for the award in 2014.

## References

- Ajala, O.E., Aberuagba, F., Odetoye, T.E., Ajala, A.M., 2015. Biodiesel: Sustainable Energy Replacement to Petroleum-Based Diesel Fuel - A Review. *ChemBioEng Reviews*, Volume 2(3), pp.145–156
- Alvarez-galvan, M.C., Campos-martin, J.M., Fierro, J.L.G., 2019. Transition Metal Phosphides for the Catalytic Hydrodeoxygenation of Waste Oils into Green Diesel. *Catalysts*, Volume 9(3), p. 293
- Ameen, M., Tazli Azizan, M., Yusup, S., Ramli, A., Yasir, M., Kaur, H., Kin Wai, C., 2019. HY Zeolite as Hydrodeoxygenation Catalyst for Diesel Range Hydrocarbon Production From Rubber Seed Oil. *Materials Today: Proceedings*, Volume 16, pp. 1742–1749
- Ameen, M., Tazli, M., Yusup, S., Ramli, A., Yasir, M., 2017. Catalytic Hydrodeoxygenation of Triglycerides: An Approach to Clean Diesel Fuel Production. *Renewable and Sustainable Energy Reviews*, Volume 80, pp. 1072–1088
- Arun, N., Sharma, R. V., Dalai, A.K., 2015. Green Diesel Synthesis By Hydrodeoxygenation Of Bio-Based Feedstocks: Strategies for Catalyst Design and Development. *Renewable and Sustainable Energy Reviews*, Volume 48, 240–255
- Chen, L., Li, H., Fu, J., Miao, C., Lv, P., Yuan, Z., 2016. Catalytic hydroprocessing of fatty acid methyl esters to renewable alkane fuels over Ni/HZSM-5 catalyst. *Catalysis today*, Volume 259, pp. 266–276
- Chen, S., Miao, C., Luo, Y., Zhou, G., Xiong, K., Jiao, Z., Zhang, X., 2018. Study of catalytic hydrodeoxygenation performance of Ni catalysts: Effects of prepared method. *Renewable Energy*, Volume 115, pp. 1109–1117
- De, S., Zhang, J., Luque, R., Yan, N., 2016. Ni-based Bimetallic Heterogeneous Catalysts for Energy. *Energy & Environmental Science*, Volume 9(11), pp. 3314–3347
- Deliy, I. V., Vlasova, E.N., Nuzhdin, A.L., Gerasimov, E.Y., Bukhtiyarova, G.A., 2014. Hydrodeoxygenation of Methyl Palmitate Over Sulfided Mo/Al<sub>2</sub>O<sub>3</sub>, CoMo/Al<sub>2</sub>O<sub>3</sub> and NiMo/Al<sub>2</sub>O<sub>3</sub> Catalysts. *Royal Society of Chemistry Advances*, Volume 4(5), pp. 2242–2250
- Dwiatmoko, A.A., Seo, J., Choi, J., Jin, D., Jae, J., Ha, J.-M., 2019. Improved Activity of a CaCO<sub>3</sub> - Supported Ru Catalyst for the Hydrodeoxygenation of Eugenol as a Model Lignin-Derived Phenolic Compound. *Catalysis Communications*, Volume 127, pp. 45–50
- Gamliel, D.P., Baillie, B.P., Augustine, E., Hall, J., Bollas, G.M., Valla, J.A., 2018. Nickel Impregnated Mesoporous USY Zeolites for Hydrodeoxygenation of Anisole. *Microporous and Mesoporous Materials*, Volume 261, pp. 18–28
- Gousi, M., Andriopoulou, C., Bourikas, K., Ladas, S., Sotiriou, M., Kordulis, C., Lycourghiotis, A., 2017. Green Diesel Production Over Nickel-Alumina Co-Precipitated Catalysts. *Applied Catalysis A: General*, Volume 536, pp. 45–56
- Hachemi, I., Kumar, N., Mäki-Arvela, P., Roine, J., Peurla, M., Hemming, J., Salonen, J., Murzin, D.Y., 2017. Sulfur-free Ni Catalyst for Production of Green Diesel by Hydrodeoxygenation. *Journal of Catalysis*, Volume 347, pp. 205–221
- Hermida, L., Abdullah, A.Z., Mohamed, A.R., 2015. Deoxygenation of Fatty Acid to Produce Diesel-Like Hydrocarbons: A Review of Process Conditions, Reaction Kinetics and

- Mechanism. *Renewable and Sustainable Energy Reviews*, Volume 42, pp. 1223–1233
- Hongloi, N., Prapainainar, P., Seubsai, A., Sudsakorn, K., Prapainainar, C., 2019. Nickel Catalyst with Different Supports for Green Diesel Production. *Energy*, Volume 182, pp. 306–320.
- Hou, L., Du, W., Qu, M., Wang, X., Wang, S., Shi, S., 2018. Self-Assembled Nickel Nanoparticles Supported on Mesoporous Aluminum Oxide for Selective Hydrogenation of Isophorone. *Asian Journal of Organic Chemistry*, Volume 7(4), pp. 757–762
- Inokawa, H., Nishimoto, S., Kameshima, Y., Miyake, M., 2010. Difference in the Catalytic Activity of Transition Metals and Their Cations Loaded in Zeolite Y for Ethanol Steam Reforming. *International journal of hydrogen energy*, Volume 35(21), pp. 11719–11724
- Kaewmeesri, R., Srifa, A., Itthibenchapong, V., Faungnawakij, K., 2015. Deoxygenation of Waste Chicken Fats to Green Diesel Over Ni/Al<sub>2</sub>O<sub>3</sub>: Effect of Water and Free Fatty Acid Content. *Energy and Fuels*, Volume 29(2), pp. 833–840
- Lani, N.S., Ngadi, N., Yahya, N.Y., Rahman, R.A., 2016. Synthesis, Characterization And Performance of Silica Impregnated Calcium Oxide as Heterogeneous Catalyst in Biodiesel Production. *Journal of Cleaner Production*, Volume 146, pp. 116–124
- Liu, J., Li, C., Wang, F., He, S., Chen, H., Zhao, Y., Wei, M., Evans, D.G., Duan, X., 2013. Enhanced Low-Temperature Activity of CO<sub>2</sub> Methanation Over Highly-Dispersed Ni/TiO<sub>2</sub> Catalyst. *Catalysis Science & Technology*, Volume 3(10), pp. 2627–2633
- Liu, J., He, J., Wang, L., Li, R. (2016). NiO-PTA Supported on ZIF-8 as a Highly Effective Catalyst for Hydrocracking of Jatropha Oil. *Scientific Reports*, 6(1), pp. 23667
- Liu, Q., Zuo, H., Zhang, Q., Wang, T., Ma, L., 2014. Hydrodeoxygenation of Palm Oil to Hydrocarbon Fuels Over Ni/SAPO-11 Catalysts. *Chinese journal of catalysis*, Volume 35(5), pp. 748–756
- Ma, B., Zhao, C., 2015. High-grade Diesel Production by Hydrodeoxygenation of Palm Oil Over a Hierarchically Structured Ni/HBEA Catalyst. *Green Chemistry*, Volume 17(3), pp. 1692–1701
- Mardiana, S., Azhari, N.J., Ilmi, T., Kadja, G.T.M., 2022. Hierarchical Zeolite for Biomass Conversion to Biofuel: A review. *Fuel*, Volume 309, p. 122119
- Muharam, Y., Soedarsono, J.A., 2020. Hydrodeoxygenation of Vegetable Oil in a Trickle Bed Reactor for Renewable Diesel Production. *International Journal of Technology*, Volume 11(7), pp. 1292–1299
- Primo, A., Garcia, H., 2014. Zeolites as Catalysts in Oil Refining. *Chemical Society Reviews*, Volume 43(22), pp. 7548–7561
- Putra, R., Lestari, W.W., Wibowo, F.R., Susanto, B.H., 2018. Fe/Indonesian Natural Zeolite as Hydrodeoxygenation Catalyst in Green Diesel Production from Palm Oil. *Bulletin of Chemical Reaction Engineering & Catalysis*, Volume 13(2), pp. 245–255
- Robinson, A.M., Hensley, J.E., Will Medlin, J., 2016. Bifunctional Catalysts for Upgrading of Biomass-Derived Oxygenates: A Review. *American Chemical Society Catalysis*, Volume 6(8), pp. 5026–5043
- Setiawan, Y., Mahatmanti, F.W., 2018. *Preparasi dan Karakterisasi Nanozeolit dari Zeolit Alam Gunungkidul dengan Metode Top-Down*. *Indonesian Journal of Chemical Science*, Volume 7(1), pp. 43–49
- Shafaghat, H., Man, J., Lee, I., Jae, J., Jung, S., Park, Y., 2018. Catalytic Hydrodeoxygenation of Crude Bio-Oil in Supercritical Methanol Using Supported Nickel Catalysts. *Renewable Energy*, Volume 144, pp. 159–166
- Thommes, M., Kaneko, K., Neimark, A.V., Olivier, J.P., Rodriguez-Reinoso F., Rouquérol, J., Sing, K. S. W., 2015. Physisorption of Gases, with Special Reference to The Evaluation

- of Surface Area and Pore Size Distribution (IUPAC Technical Report). *Pure and Applied Chemistry*, Volume 87, pp. 1051–1069
- Srifa, A., Faungnawakij, K., Itthibenchapong, V., Assabumrungrat, S., 2015. Roles of Monometallic Catalysts in Hydrodeoxygenation of Palm Oil To Green Diesel. *Chemical Engineering Journal*, Volume 278, pp. 249–258
- Srifa, A., Kaewmeesri, R., Fang, C., Itthibenchapong, V., Faungnawakij, K., 2018. NiAl<sub>2</sub>O<sub>4</sub> spinel-type catalysts for deoxygenation of palm oil to green diesel. *Chemical Engineering Journal*, Volume 345, pp. 107–113
- Susanto, B.H., Prakasa, M.B., Nasikin, M., Sukirno, 2016. Synthesis of Renewable Diesel from Palm Oil and Jatropha Curcas Oil Through Hydrodeoxygenation Using Nimo/ZAL. *International Journal of Technology*, Volume 7(8), pp. 1404–1411
- Taromi, A.A., Kaliaguine, S., 2018. Green Diesel Production via Continuous Hydrotreatment of Triglycerides over Mesostructured  $\Gamma$ -Alumina Supported Nimo/Como Catalysts. *Fuel Processing Technology*, Volume 171, pp. 20–30
- Xin, H., Guo, K., Li, D., Yang, H., Hu, C., 2016. Production of High-Grade Diesel From Palmitic Acid over Activated Carbon-Supported Nickel Phosphide Catalysts. *Applied Catalysis B: Environmental*, Volume 187, pp.375–385
- Yang, J., Li, S., Zhang, L., Liu, X., Wang, J., Pan, X., Li, N., Wang, A., Cong, Y., Wang, X., Zhang, T., 2017. Hydrodeoxygenation of Furans over Pd-Fe<sub>x</sub>/SiO<sub>2</sub> Catalyst under Atmospheric Pressure. *Applied Catalysis B: Environmental*, Volume 201, pp. 266–277
- Yang, L., Tate, K.L., Jasinski, J.B., Carreon, M.A., 2015. Decarboxylation of Oleic Acid to Heptadecane over Pt Supported on Zeolite 5A Beads. *American Chemical Society Catalysis*, Volume 5(11), pp. 6497–6502
- Yang, Y., Ochoa-Hernández, C., De La Peña O'Shea, V.A., Coronado, J.M., Serrano, D.P., 2012. Ni<sub>2</sub>P/SBA-15 as a Hydrodeoxygenation Catalyst with Enhanced Selectivity for the Conversion of Methyl Oleate Into N-Octadecane. *American Chemical Society Catalysis*, Volume 2(4), pp. 592–598
- Yulizar, Y., Kadja, G.T.M., Safaat, M., 2016, Well-Exposed Gold Nanoclusters on Indonesia Natural Zeolite: A Highly Active and Reusable Catalyst for the Reduction of P-Nitrophenol. *Reaction Kinetics, Mechanisms and Catalysis*, Volume 117, pp. 353-363
- Yuswan, M., Adinda, D.P., Muharam, Y., Soedarsono, J.A., Susanto, B.H., Prakasa, M.B., Nasikin, M., Sukirno, 2018. Simulation of Hydrotreating of Vegetable Oil in a Slurry Bubble Column Reactor for Green Diesel Production. *International Journal of Technology*, Volume 9(6), pp. 1168–1177
- Zuo, H., Liu, Q., Wang, T., Ma, L., Zhang, Qi, Zhang, Qing, 2012. Hydrodeoxygenation of Methyl Palmitate over Supported Ni Catalysts for Diesel-Like Fuel Production. *Energy and Fuels*, Volume 26, 3747–3755